Research Article

Simulation of the response of a segmented high-purity germanium detector for gamma emission tomography of nuclear fuel

Peter Andersson[1] · Vikram Rathore[1] · Lorenzo Senis[1] · Anastasios Anastasiadis[1] · Erik Andersson Sundén[1] · Haluk Atak[2] · Scott Holcombe[3] · Ane Håkansson[1] · Peter Jansson[1] · Johan Nyberg[1]

Received: 18 October 2019 / Accepted: 15 January 2020

Abstract
Irradiation testing of nuclear fuel is routinely performed in nuclear test reactors. For qualification and licensing of accident-tolerant fuels or generation IV reactor fuels, an extensive increase in irradiation testing is foreseen in order to fill the gaps of existing validation data, both in normal operational conditions and in order to identify operational limits. Gamma emission tomography (GET) has been demonstrated as a viable technique for studies of the behavior of irradiated nuclear fuel, e.g., measurement of fission gas release and inspection of fuel behavior under loss-of-coolant accident conditions. In this work, the aim is to improve the technique of GET for irradiated nuclear fuel, by developing a detector concept that allows for a higher spatial resolution and/or faster interrogation. We present the working principles of a novel concept for gamma emission tomography using a segmented high-purity germanium (HPGe) detector. The performance of this concept was investigated using the Monte Carlo particle transport code MCNP. In particular, the data analysis of the proposed detector was evaluated, and the performance, in terms of full energy efficiency and misidentification rate (i.e., localization failure), was assessed. We concluded that the segmented HPGe detector has an advantageous performance as compared to the traditional single-channel detector systems. Due to the scattering nature of gamma rays, a trade-off is presented between efficiency and cross-talk; however, the performance is nevertheless a substantial improvement over the currently used single-channel HPGe detector systems.

Keywords Post-irradiation examination · Gamma emission tomography · Nuclear fuel · Segmented high-purity germanium detector · Gamma spectroscopy · Irradiation testing

1 Introduction

Irradiation testing for development and licensing of nuclear fuel is routinely performed in several nuclear test reactors in the world. Typically, nuclear fuel rodlets are irradiated, where the dimensions of the fuel, e.g., the pellets, mimic the fuel products used in the nuclear industry. Currently, programs such as fission accelerated steady state test (FAST) [1] demonstrate a trend toward the irradiation testing of smaller fuel samples. This could accelerate the testing phase of nuclear fuel for advanced reactors and of accident-tolerant fuels. However, such programs may require adaptation of post-irradiation examination infrastructures, in order to handle high throughput of small nuclear fuel samples.

Gamma emission tomography (GET) is a nondestructive and non-intrusive technique for assay of the internal composition of an object under investigation. In GET, external measurements are performed to map the gamma-ray field

✉ Peter Andersson, peter.andersson@physics.uu.se | [1]Department of Physics and Astronomy, Uppsala University, Uppsala, Sweden. [2]Department of Nuclear Engineering, Hacettepe University, Ankara, Turkey. [3]Department of Nuclear Fuels and Materials Experiments, Institute for Energy Technology, Halden, Norway.

SN Applied Sciences (2020) 2:271 | https://doi.org/10.1007/s42452-020-2053-4

Published online: 25 January 2020

from the object under study. From this intensity map, the internal distribution of the activity is reconstructed.

In recent years, various devices have been designed and operated in order to implement the GET technique for applications within nuclear safeguards [2, 3], and for validation of power and burnup distributions [4–7]. In collaboration between Uppsala University, the OECD Halden Reactor Project and Westinghouse Electric Sweden, a gamma emission tomography instrument was recently designed, constructed and operated at the Halden boiling water reactor (HBWR) to allow for nondestructive studies of irradiated test fuel [8, 9].

The required components of a GET system are a collimated detector (or multiple detectors) and an arrangement for translational and rotational movements of the detector(s) around the measurement object. In the case of the Halden GET system, a single HPGe detector is used, as shown in Fig. 1. The detector is used to make a spectrometric assessment of the activity distribution of selected gamma-emitting radionuclides in the fuel rig. These inspections are performed without disassembling the fuel rods from the test rig. With a GET system located on the reactor site, it also offers to reduce the handling and transportation time that would often be required by alternative post-irradiation examination techniques, and it facilitates the reinsertion of the fuel test rig into the reactor core for further irradiation, if desired. For a more thorough description of a GET system for nuclear fuel, we refer to Ref. [8] about the Halden GET system.

2 Scope and motivation

Spatial-resolution requirements of a GET system for the examination of nuclear fuel depend on the imaging task. In the Halden GET system, the collimator in between the detector and the fuel rods can be exchanged and the translation step size of the stepping motor can be varied in order to obtain various spatial resolutions. While the ultimate limit of achievable resolution is difficult to evaluate, the smallest collimator that was used until now has a 1-mm-wide slit, which was used in 1 mm lateral scan steps. Consequently, the best resolution obtained was also in the order of 1 mm [10].

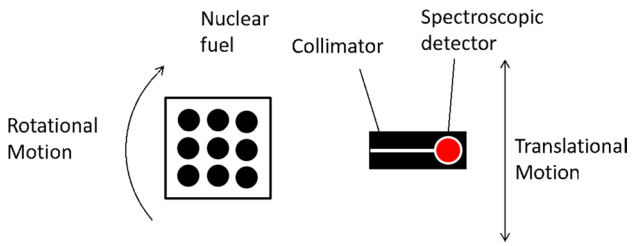

Fig. 1 Schematics of a GET system. The setup includes a radioactive irradiated fuel (left), a collimated gamma-ray detector (right). The gamma-ray intensity is measured with repeated rotational and translational steps of the object relative to the detector. It can be noted that similar systems may operate submerged in water for shielding and cooling of the fuel [2, 4] or in air [6, 8]

The aim of this work is to achieve better spatial resolution of the GET technique in order to facilitate imaging of rod-internal features, and interrogation of smaller irradiated fuel samples. The desired outcome of this work is to obtain spatial resolution of a GET system in the order of 0.1 mm, i.e., one order of magnitude improvement over the previous system. This may facilitate studies of properties/phenomena such as

- Fission product migration [8],
- Fission gas release measurements [11],
- Pellet cladding interactions,
- Rod bow and swelling,
- Fuel fragmentation, relocation and dispersal in transient tests such as LOCA [12],
- Rod-internal burnup and power distribution,
- Studies of small fuel samples for accelerated irradiation testing.

In principle, in order to obtain better spatial resolution data, a narrower collimator slit may be utilized and scans of smaller stepping intervals may be performed. However, this would increase the measurement time requirements of the interrogation due to the large number of measurements required and due to the decreased flux on the detectors. Therefore, in order to obtain high spatial resolution without adverse effects on the measurement time, there is a need to compensate for the loss of efficiency when using smaller collimators. For this purpose, a variety of options are available that may be considered independently or in combination, such as optimization of collimator length, using a high aspect ratio (height/width) of the collimator slit, shortened cooling time between end of irradiation and the start of interrogation, and by using multiple detectors or detector channels.

In this paper, we propose the use of a segmented HPGe detector for achieving a multichannel GET detector. The performance of the detector was investigated using Monte Carlo simulations, and the predicted performance was compared with a single-channel HPGe detector, such as used in the Halden GET system.

3 Proposed detector concept

The proposed concept is to use electronically segmented coaxial HPGe detectors. Such detectors consist of monolithic germanium crystal with one of the contact electrodes

(outer one in the proposed detector) segmented in order to obtain spatially resolved readout. In effect, a single HPGe crystal together with a multislit collimator thus creates multiple collimated lines of sight through the fuel object.

Due to current manufacturing limitations, the segments must be at least about 5 mm wide [13], which restricts the number of collimator slits to two per cm. High spatial resolution can be achieved by repeated measurements with sub-millimeter offset interval of the detector–collimator system.

Segmented HPGe detectors are used when position sensitivity of the detected gamma rays is required [14]. In the gamma-ray tracking spectrometers AGATA and GRETINA [15–17], the gamma-ray interactions are localized in 3D in segmented HPGe detectors by performing pulse-shape analysis based on a combination of three different methods: (a) identification of the net pulse signal in the segmented electrodes, (b) comparison of mirror pulse amplitudes in neighboring segments and (c) the use of pulse shape in the rising slope of the net pulse. In addition, there are applications of segmented detectors in solar and astrophysics [18, 19] as well as in nuclear security for identification of nuclear materials [20].

In the context of our work, where 1D information of the first interaction of the photon in the detector suffices to identify the entrance collimator slit, the main track is to make use of method (a) above, i.e., identification of the segment electrode that produced a net pulse. For this purpose, we may segment a coaxial crystal along the axial direction and align each axial segment with a slit of the collimator. Due to a limitation on the maximum outer dimensions of the coaxial detectors of approximately 90 mm long and 80 mm in diameter [13], the number of axial segments is at most 90 mm/5 mm = 18.

As the gamma-ray photons are likely to undergo multiple scattering interactions before photoelectric absorption, neighboring segments may be hit by scattered gamma-ray photons producing an interfering signal. In our proposed detector concept, the problem of scattering for the localization of the first interaction is mitigated using azimuthal segmentation in addition to the axial, as shown in Figs. 2 and 3. The purpose of the two large azimuthal segments is to absorb the scattered gamma rays while being outside of the direct beams from the multislit collimator. The interactions in the large azimuthal segments can therefore be excluded from being the first interaction of the gamma ray. By this approach, the collimator slit of origin can be identified, if only one scattering segment is triggering. The two large azimuthal segments are henceforth referred to as energy deposition segments, while the detector segments aligned with the collimator slits are referred to as scattering segments. Based on the motivations above, in total our proposed detector has 38 segments: 18×2 scattering segments (the factor of two corresponds to the pair of segments needed to cover the

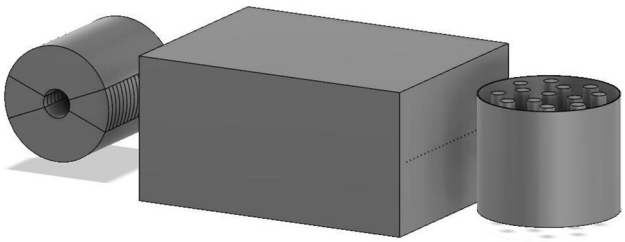

Fig. 3 Schematic drawing of the detector concept showing also the location of a multislit collimator and a fuel object. Note that, e.g., cryostat, preamplifiers, cabling and shielding are excluded from the drawing. Left: segmented coaxial HPGe detector. Middle: collimator. Right: irradiated fuel rig with test rods

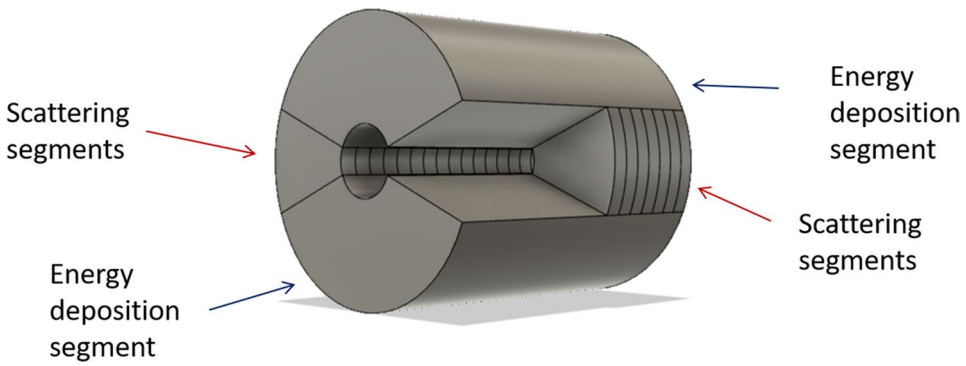

Fig. 2 Cutout view of the proposed detector concept. An HPGe crystal of true coaxial geometry with (electronic) segmentation in four azimuthal zones, two of which are intended for localization of the first interaction of the gamma ray (scattering segments), and two are intended for capturing the energy deposition of subsequent gamma-ray interactions (energy deposition segments). The scattering segments are segmented in the axial direction; each pair of scattering segments is aligned with one slit of the collimator, see Fig. 3

front and back sides) and two energy deposition segments (upper and lower).

4 Readout and analysis

The planned mode of analysis for the segmented detector is that each segment is separately read out by a high-speed digitizer channel on one of their electrodes, while one common digitizer channel is dedicated to the core (central) electrode, which is shared by all segments. There is in total a need for 39 digitizer channels, of which 36 are for the scattering segments, two for the energy deposition segments and one for the core, shared for all the segments. The layout of the electrodes is shown in Fig. 4.

For the analysis, a trigger level signal is proposed on the unsegmented core contact. Therefore, low-energy events of no interest to the fuel inspection, e.g., background signals, can be discarded without unnecessarily occupying data storage. Note that events scattering in multiple segments will still give a signal in the core electrode that is proportional to the total deposited energy.

For triggering events, the number of activated scattering segments is examined. If only one scattering segment was triggered, the allocation of the event to the corresponding collimator slit of entry is trivial. However, due to the possibility of energy deposition in multiple scattering segments, some events may need to be discarded to avoid misidentification of the position of the initial interaction, when multiple scattering segments are triggered.

For the analysis of the such data, we have evaluated two suggested methods to obtain source position, method (1) by associating each event with the entrance scattering segment where the largest energy deposition took place, as previously done in Ref. [18], and method (2) by discarding any events where energy was deposited in multiple scattering segment pairs. In the latter method, the efficiency is adversely impacted due to vetoing many of the potential photon tracks. However, the misidentification probability should be substantially lower, since when in doubt, the event is discarded.

In addition, as a compromise between methods 1 and 2 above, the use of a secondary trigger has been considered, where the event is counted in the segment where the largest energy was deposited, unless the energy deposited in any other segment surpasses a selected trigger level.

5 Simulation study of proposed detector concept

Using the Monte Carlo radiation transport code MCNPX2.5 [21], the interactions of gamma rays in the proposed detector concept were studied. The F8 pulse height tally was used to achieve simulated energy deposition spectra. However, in order to simulate the analysis according to methods 1 and 2 described above in Sect. 3, where coincidence and anticoincidence energy deposition events in the various detector segments were needed, the event-to-event distribution of energy in the individual detector segments was tracked with the PTRAC function. This function creates output tables of all relevant parameters, such as energy, position and direction of the photon for every tracked event. These tables were post-processed by summing of all energy deposited in each segment of the detectors for each

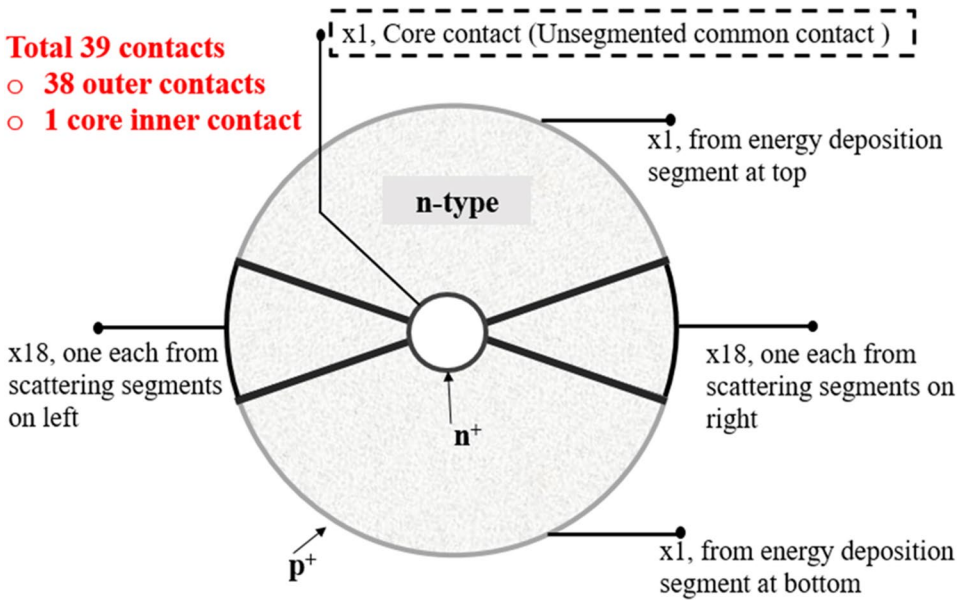

Fig. 4 Electrode configuration and segmentation pattern of the proposed detector

individual photon. The post-processing was used to mimic the analysis according to methods 1 and 2.

The probability, p, of the photons to satisfying the conditions used for methods 1 or 2 is estimated based on the number of successful trials, s, and the total number of trials, n, such that $p = s/n$. The 1σ precision was calculated under the assumption that it follows the binomial distribution, i.e., $\sigma = \sqrt{np(1-p)}$.

The coaxial detector used in the simulation had an inner diameter of 14 mm, outer diameter of 80 mm and the length of 90 mm. The scattering segments consist of two opposing segments shaped like pie slices, each with a central angle of 36.9°. This implies that the two energy deposition segments each have a central angle of 143.1°. Furthermore, the thickness of the scattering segments was 5 mm.

5.1 Detection efficiency test

The intrinsic full energy detection efficiency, i.e., the probability of an incident photon to be detected in the full energy peak, was studied using monodirectional photon beams incident on each detector segment. 3×10^8 starting photons were used in the simulation, and the fraction of the histories which deposited the full energy in the detector crystal was used as an estimate of the intrinsic full energy efficiency. The source, located at a distance of 10 cm from the detector center, was modeled as a point source, and source biasing was used to direct the photon beam toward the collimator. The gamma-ray energy was 662 keV, chosen to represent the gamma ray following the decay of Cs-137.

5.2 Trade-off between misidentification rate and detection efficiency

Since the interaction and energy distribution across the segments can be described as random processes, method 1 will not be fail safe, but rather there is a finite chance of misidentification of the initial interaction. In this study, the frequency of misidentification was evaluated, as well as the detection efficiency. The use of the secondary trigger level mentioned above in Sect. 4 was explored, where the energy in the segment with the second largest energy deposition must not exceed the trigger level, or otherwise the event is discarded. The misidentification rate and the full energy efficiency were investigated when varying the secondary trigger level.

5.3 Evaluation of localization using methods 1 and 2 for distributed gamma-ray source in shielded geometry

Finally, to investigate the performance of the detector system in a realistic case, a simulation was performed with an extended source emitting gamma rays with several energies. In this investigation, the detector crystal was placed inside an aluminum shroud (1.5 mm thick) and substantial amounts of densimet® (tungsten alloy) shielding in order to provide a realistic scattered photon background. See the geometry from the MCNP model in Fig. 5.

The source was extended spatially in discrete points in front of three of the collimator slits, arbitrarily selected as number 8, 9 and 14. In addition, the source energy distribution included four gamma energies of 662 keV, 1173 keV, 1332 keV and 1596 keV. This test spectrum corresponds to the dominant gamma lines from the decays of Cs-137, Co-60 and La-140, all of which are relevant to

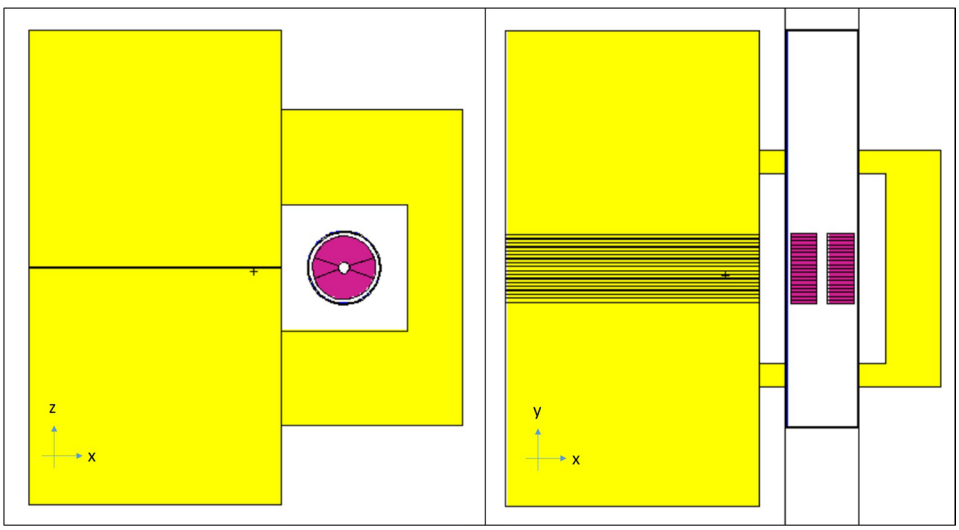

Fig. 5 Left and right: the MCNP simulation geometry in the test of spectral response and localization methods. Purple: germanium detector. Yellow: shielding and collimator absorber of tungsten alloy. Blue: aluminum shroud. The source was located to the left of the 18-slit collimator. The collimator slits are rectanguloids with the dimensions $W{:}H{:}L = 0.4$ mm:1 mm:320 mm

spectrometry of irradiated nuclear fuel. The intrinsic detection efficiency and the misidentification rate (i.e., failure to localize the first interaction to the right segment) were investigated for methods 1 and 2 using PTRAC output tables.

To speed up the convergence of the simulation results, the source was biased to only emit particles within a 6° angle from the orientation of the slits, i.e., the source was biased in the forward direction toward the detector, which results in more simulated photon tracks to reach the detector. The angular spread was selected big enough to irradiate the entire height and width of the collimator slit openings on the side facing the object. It can be noted that the intrinsic efficiency is normalized by the number of incident photons in the detector, and the misidentification rates are normalized per full energy event in the detector, and therefore, these estimated quantities do not need to be compensated for the source biasing.

The entrance slit of the source event was tagged in the analysis of the PTRAC file by use of the spatial coordinates of the source event. This was in turn compared to the identified location of the event, using the suggested approaches (methods 1 and 2 described in Sect. 4), but with the simulated energy deposition according to the PTRAC output in each segment as a surrogate for the measured pulse height.

6 Simulation results

6.1 Detection efficiency

The intrinsic full energy efficiency in the central detector channel (defined by two opposing scattering segments in the center of the crystal, in union with the two energy deposition segments) was estimated for 662 keV photons. The estimate was based on the probability of full energy deposition in the concerned segments using the F8 tally, i.e., thereby excluding all energy deposited in other scattering segments from the calculation of the pulse height. The energy deposition distribution in these segments is shown in Fig. 6, and the probability of full energy deposition in the concerned segments was found to be 27.778(3)%. This corresponds to the intrinsic full energy efficiency of the proposed detector according to analysis method 2, described above in Sect. 4. The total spectrum efficiency was also estimated, where 91.212(2)% of the gamma rays interacted in the crystal and contributed to the spectrum. The total spectrum efficiency can be easily be confirmed using the linear attenuation law, where the transmission, T, equals $I/I_0 = e^{-\mu\Delta x}$, where μ is the total attenuation coefficient without coherent scattering for germanium according to [22], and $\Delta x = 66$ mm is the traversed distance in the germanium. The total spectrum efficiency is $1-T = 91.28\%$. This is in relatively good agreement with our obtained efficiency using MCNP.

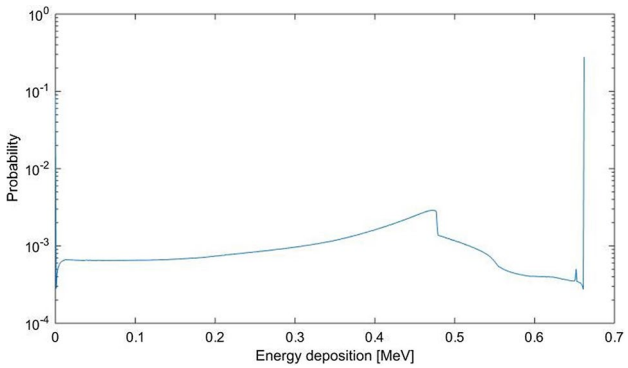

Fig. 6 Energy deposition distribution of 662 keV gamma rays in the proposed detector concept (in the target scattering segments and the two energy deposition segments). The central scattering segment pair was targeted by the beam. Note the zero bin to the left which indicates photons transmitted without interaction in the detector. The full energy bin (far right) was used to calculate the fraction of full energy depositions of the 3×10^8 starting histories

The variability of the detection efficiency was examined over the scattering segments. Nine of the 18 segments were studied due to symmetry, and the efficiency was found to decrease toward the edges of the detector, since scattered photons in the outermost segments are more likely to escape the detector before complete absorption. The maximum efficiency of 28% was registered in the center, while the lowest efficiency of 19% was registered at the edge scattering segment. The trend is shown in Fig. 7.

6.2 Trade-off between efficiency and misidentification rate

In Sect. 6.1, the reported detection efficiency was based on method 2, i.e., energy deposition in only one of the scattering segment pairs, in which case localization of the corresponding slit of entrance is trivial. However, the detection efficiency can be increased according to method 1, where determination of the segment of the first interaction is attempted, by appointing the point of origin to the scattering segment with the largest energy deposition. Therefore, some events are also misplaced using this assumption.

The intrinsic full energy efficiency and the misidentification rate were investigated for methods 1 and 2 for a test case of 662 keV gamma rays. In addition to the two methods, a trigger level was applied on the deposition in the scattering segment of the second largest signal. If the trigger level was reached, the event was discarded, and correspondingly, if the deposition in the second

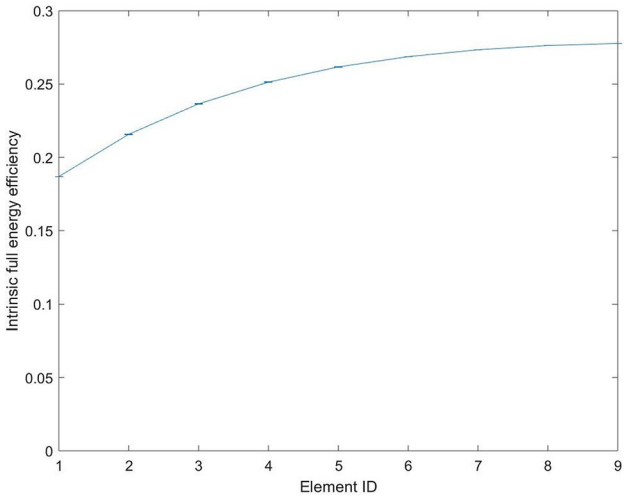

Fig. 7 Variation in the intrinsic full energy efficiency over the detector concept. Element 1 is the outermost segment, and element 9 is one of the two center segments

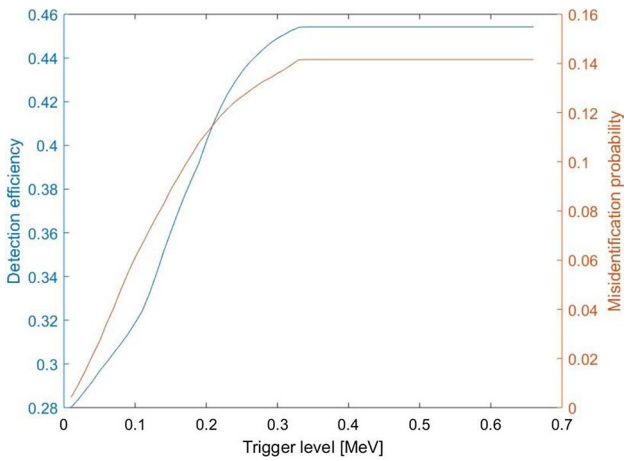

Fig. 8 Intrinsic full energy efficiency (left axis) and misidentification rate (per full energy event) (right axis) for 662 keV photons and secondary trigger level on *x*-axis. Note that the secondary trigger level is applied to the scattering segment with the second largest energy deposition, and if the trigger level is reached, the pulse is discarded

segment is less than the selected trigger level, the event is counted and localized to the segment with the largest energy deposition. It can be noted that setting the trigger level to zero is equivalent to using method 2, while setting it to infinity is equivalent to method 1. For values between these extremes, the trigger level corresponds to a compromise between the two. The variation in detection efficiency and misidentification rate is shown in Fig. 8. As expected, the efficiency increases for a higher secondary trigger, and in addition, the probability of misidentification increases.

6.3 Test of slit identification procedure with distributed source

The final simulation source included a distributed gamma source of four gamma energies (662, 1173, 1332 and 1596 keV) positioned at three different collimator slits, as well as a realistic scattering environment from the collimator and shielding. Of the total 4×10^9 simulated source photons, 1.5×10^5 found their way to the detector, and for these, all tracked events (numbering to 3×10^6 in total) were printed in the MCNP PTRAC output file.

The total detector energy deposition spectrum is shown in Fig. 9 for analysis method 1 (counting all events and attempting localization), while Fig. 10 shows the spectrum when applying method 2 (discarding events with deposition in multiple scattering segments). It can be noted that the spectra in both cases contain the full-energy absorption lines superimposed on scattered background continua, which is qualitatively similar to what is expected when using conventional analysis methods, i.e., without any coincidence or anticoincidence filters.

For a test of the slit localization methods on the relatively realistic spectra modeled in this simulation, methods 1 and 2 were tested on the events that deposited in the full energy peak. Here, the analysis included the full energy ±2 keV to account for a region of interest used for the peak analysis. Subsequently, the PTRAC output was examined by counting the number of misidentified first interaction locations, and evaluating the corresponding rate. It was found that using method 1, a relatively large fraction of the gamma rays was incorrectly localized, from 7 to 15%. The misidentification rate is stated in Table 1 for the four gamma energies used.

A closer inspection of the misidentified events of method 1 was performed, where the as-localized position was found mostly to be one of the neighboring segments to the correct position. The distribution of all identified locations for method 1 is shown in Fig. 11.

In the case of method 2, the problem of incorrect localization is largely mitigated. For all four energies, more than 99.7% of the counted events were correctly localized. It can be noted, however, that 16 events with full energy deposition were erroneously localized even with the safer analysis according to method 2. The misidentified events were caused by coherent scattering in the first interaction in the detector. Therefore, the full energy could be deposited elsewhere in the detector, and consequently, it lead to full energy events being misidentified.

Some misidentifications were also caused by the first scattering interaction of the photon not taking place in the detector crystal, but instead in, e.g., the collimator, the aluminum shroud covering the detector, or the shielding behind the detector (backscattering). However, all these

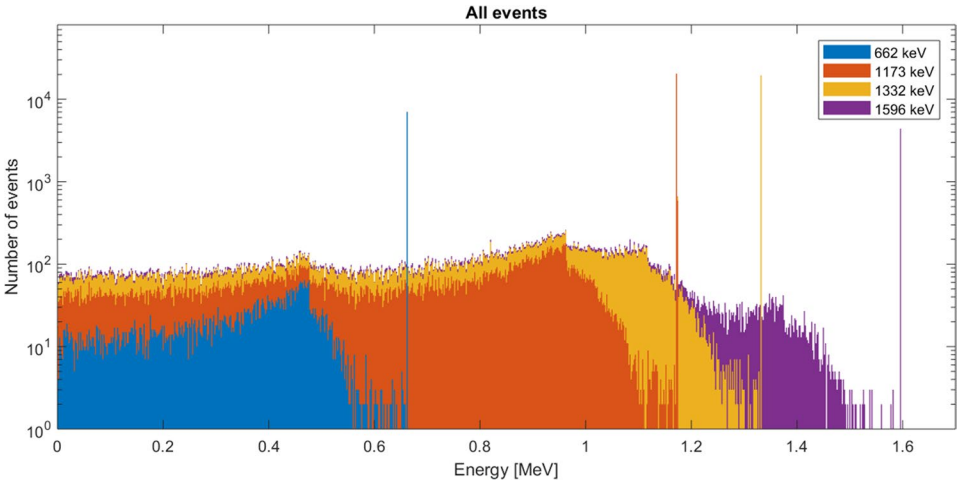

Fig. 9 Total spectrum, all segments. The stacked color bars represent the initial energy of the photon. In this spectrum, all events are shown, corresponding to method 1 of the data analysis description in Sect. 3

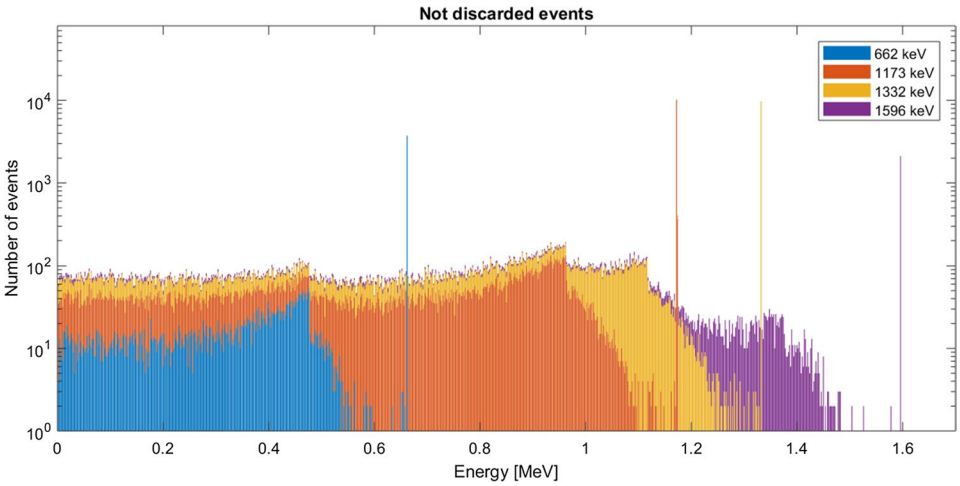

Fig. 10 Stacked histogram of the energy deposition in the detector. This spectrum contains only photon histories that passed the veto, where any coincident events in multiple scattering sections are discarded (i.e., method 2 of Sect. 3)

Table 1 Misidentification rate and the full energy efficiency for the four evaluated gamma-ray energies. Note that the misidentification rates were normalized per full energy deposition. 1σ uncertainties in parenthesis were calculated as described in Sect. 5

Gamma-ray energy	Misidentification rate (method 1) (%)	Full energy efficiency (method 1) (%)	Misidentification rate (method 2) (%)	Full energy peak efficiency (method 2) (%)
662 keV	15.0 (4)	42.5 (4)	0.22 (8)	26.3 (3)
1173 keV	9.2 (2)	32.9 (2)	0.04 (2)	18.1 (2)
1332 keV	8.4 (2)	30.4 (2)	0.04 (2)	16.5 (2)
1596 keV	7.3 (4)	27.5 (4)	0 (0)	14.3 (3)

events had lost energy outside the detector and did therefore not interfere with the spectrometric assessment of the full energy peak. They may, however, still interfere with other lower-energy peaks and contribute to the pileup and dead time.

6.4 Performance of the segmented detector compared to a single-channel detector system

The aim of the current work is to develop a multichannel detector system comprised of a segmented HPGe

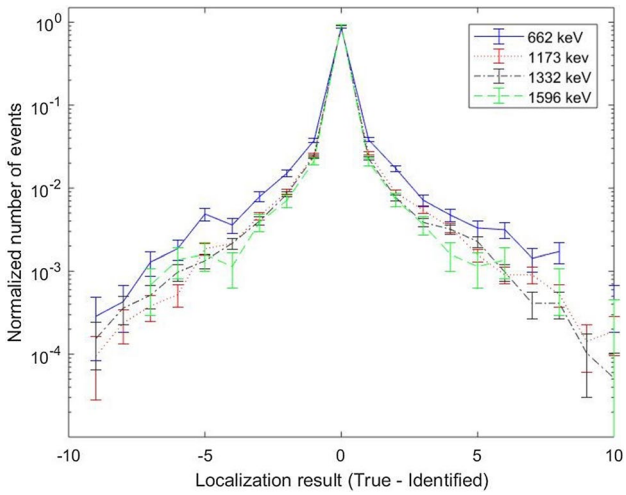

Fig. 11 Result of the localization procedure according to method 1. The localization result on the *x*-axis represents the difference of the segment indices of the as-identified location and the true location (zero if correct). The misidentified events appear mostly in the neighboring segments. As seen, the higher the gamma-ray energy, the larger the probability of correct localization

detector, such as to allow high-resolution GET by increasing the data collection rate. As seen in Table 2, the overall data collection rate for our proposed detector concept is much faster than the previous instrument used in the Halden reactor, since 18 detector channels can be utilized simultaneously in the proposed system.

There is an adverse effect of cross-talk between channels on the detection efficiency (if method 2 described above is used). However, it is a relatively minor decrease; the full energy efficiency of the proposed detector was estimated to be 25% on average of the 18 segments, whereas the currently used system has a single channel with an efficiency of 32%.

7 Conclusions

A segmented HPGe detector concept has been proposed for usage in a spatially resolved detector for gamma emission tomography of nuclear fuel. HPGe detectors have well-known good performance in terms of energy resolution, allowing for spectral analysis of complex gamma-ray spectra from nuclear fuel. The proposed detector is electronically segmented into two conceptually different segment types, scattering segments that are aligned with the collimator slits in order to identify the location of the first interaction, and energy deposition segments that are located outside the collimated beams, in order to improve the full energy deposition rate.

Two data analysis methods (1 and 2) were developed for the identification of the scattering segment first interaction location, where method 1 makes use of all events, including events with cross-talk between the detector channels, by associating each event with the scattering segment of the largest energy deposition. On the contrary, in method 2 any events with cross-talk between the scattering segments are discarded. The two methods were found to present different trade-offs between efficiency and localization success rate, where method 1 has higher efficiency than method 2, and the localization success rate is higher for method 2.

The presented simulation study shows that despite the scattering nature of typical gamma-ray energies from used nuclear fuel, the segmented detector may maintain relatively high full energy efficiency, even using method 2, ranging from 19 to 28%, and increasing toward the central segments. It can be noted that this is approximately half the efficiency of the full crystal without segmentation. A notable improvement of the proposed design is the simultaneous interrogation of up to 18 channels, thereby improving the overall data collection rate with nearly one order of magnitude.

It is concluded that the segmented HPGe detector is a viable detector option for high-spatial-resolution tomography of irradiation tested fuel, where the radiation field

Table 2 Comparison of existing and proposed GET detector for nuclear fuel studies

Device	Detector (crystal size)	No. of detection elements used	Intrinsic full energy peak efficiency (662 keV), ε_p
HALDEN GET system [8]	HPGe (5 × 5 cm)	1	32.15%[a]
Proposed device	HPGe (8 × 9 cm)	18	24.98% (method 2, using the average of all channels)

[a]Calculated with MCNP simulations with the as-stated dimensions of the detection elements in [8]

from a nuclear fuel needs to be interrogated in many positions and orientations in a limited measurement time.

8 Outlook and discussion

The simulation study has shown that the segmented HPGe detector is a viable option for gamma emission tomography. However, the presented studies are based on a first iteration of the segment pattern, with regard to (most importantly) the central angle of the azimuthal segmentation and the inner diameter of the coaxial detector. Further studies are planned for addressing the optimization of these dimensions.

In addition, the collimator dimensions and the detector design will be optimized for representative cases of fuel objects and burnup histories. In particular, attention is foreseen on the compromise between achieving fast tomography interrogation and maintaining count rates below saturation levels. It is considered likely that the collimator slit dimensions used in these simulations are not final; instead, collimator dimensions may be varied, in order to adapt to various source term conditions and spatial resolution requirements.

Regarding the height of the collimator slit, one can note that increasing the aspect ratio (height/width) may be a way of mitigating loss of intensity when using smaller slit width. In many cases, nuclear fuel presents an axial symmetry (in the case of fuel rods) that may be taken advantage of, by having a high aspect ratio. However, for, e.g., fragmented fuel in transient test, or for TRISO fuel particles, such axial symmetry may not be present. Therefore, we foresee that different (or variable) collimator slit size should be used in order to best match with the varying needs that may be presented. It is expected the aspect ratio may vary from 1:1 to more than 10:1.

The detector concept can be used with the same segmentation regardless of the aspect ratio, however, with the condition that the slit dimensions do not allow for direct irradiation of a larger region than the intended target scattering segment. This causes some constraints to the collimator width and height. Specifically, the width of the collimator slit must be smaller than the segment width of 5 mm (where also some divergence of the beam needs to be considered). Otherwise, the beam will interfere with the neighbor scattering segment and the respective collimator slit. Similarly, the height of the slit must be smaller than minimum height of the scattering segments (which is at the inner electrode). The segmented detector model presented in this paper allows for about maximum 2 mm height, without causing direct irradiation of the energy deposition segments, which in turn may cause misidentification of the first interaction. Continued studies are aiming to improve the segment pattern, with regard to optimization of the central angle of the scattering segments and the central hole diameter.

Dead time and pileup problems issues are usually connected with high count rates. Since a multislit collimator leads to higher count rate than an otherwise equivalent single-slit collimator, this problem might be expected to be worse with the proposed detector concept. While this is true, the purpose of the concept is to allow for faster data collection rate in situations where very small collimator slits are used, and consequently, the typical count rates are low in the anticipated usage. In high-resolution tomography scan of high burnup and low-cooling-time LOCA test rods with the Halden tomography system [12], using a 1 by 2 mm collimator slit, the total spectrum count rates were typically lower than 1000 cps, where an HPGe detector might be expected to perform well up to the order of 100,000 cps [23]. Therefore, there is margin to increase the count rate substantially before expecting to encounter dead time or pileup issues. Still, in certain usage scenarios, with particular combinations of fuel size, burnup history and collimator slit size, the issue of dead time and pileup might limit the benefits provided by using multiple channels.

The potential consequences of neutron damage to the detector crystal have been considered and are not expected to be a critical showstopper. The reasons for this are that the HPGe detector in the Halden system has been used for many years for gamma-ray spectrometry of nuclear fuel, and it is still operating to satisfaction. While minimized collimator length may increase the neutron dose rate to the crystal, the fuels are not expected to be very different in terms of neutron source rate, and thus, we do not expect a major change compared to the Halden case. In addition, irradiation damage on HPGe systems was mitigated in the past with the use of annealing, for example in space physics applications [24]. Finally, the detector producer with which we are in contact, Mirion, has stated that their n-type detectors are commonly operating in environments where detectors need to be annealed after neutron damages, and therefore, this is an option if needed.

Acknowledgements Open access funding provided by Uppsala University. This study was funded by the Swedish Research Council, Grant Number 2017-06448, and by the Swedish Foundation for Strategic Research, Grant Number EM16-0031.

Compliance with ethical standards

Conflict of interest The authors declare that they have no conflict of interests.

References

1. Curnutt B, Beausoleil G (2019) The fission accelerated steady state test (FAST)—a revised capsule design for the accelerated testing of advanced reactor fuels. Trans Am Nucl Soc 120:293–296
2. White T, Mayorov M, Lebruin A, Peura P, Honkanmaa T, Dahlberg J, Keubler J, Ivanov V, Turunen A (2018) Application of passive gamma emission tomography (PGET) for the verification of spent nuclear fuel. In: Proceedings from INMM 59th annual meeting
3. Smith LE et al. (2016) A viability study of gamma emission tomography for spent fuel verification: JNT 1955 phase I technical report
4. Jansson P, Jacobsson Svärd S, Håkansson A, Bäcklin A (2006) A device for nondestructive experimental determination of the power distribution in a nuclear fuel assembly. Nucl Sci Eng 152:76–86. https://doi.org/10.13182/NSE06-A2565
5. Caruso S (2007) Characterisation of high-burnup LWR fuel rods through gamma tomography. Thesis
6. Caruso S, Jatuff F (2014) Design, development and utilisation of a tomography station for γ-ray emission and transmission analyses of light water reactor spent fuel rods. Prog Nucl Energy 72:49–54
7. Svärd SJ, Håkansson A, Bäcklin A, Osifo O, Willman C, Jansson P (2005) Nondestructive experimental determination of the pin-power distribution in nuclear fuel assemblies. Nucl Technol 151:70–76. https://doi.org/10.13182/NSE06-A2565
8. Holcombe S, Svärd SJ, Hallstadius L (2015) A novel gamma emission tomography instrument for enhanced fuel characterization capabilities within the OECD Halden reactor project. Ann Nucl Energy 85:837–845. https://doi.org/10.1016/j.anucene.2015.06.043
9. Andersson P, Holcombe S (2017) A computerized method (UPPREC) for quantitative analysis of irradiated nuclear fuel assemblies with gamma emission tomography at the Halden reactor. Ann Nucl Energy 110:88–97. https://doi.org/10.1016/j.anucene.2017.06.025
10. Andersson P, Holcombe S, Tverberg T (2017) Quantitative gamma emission tomography inspection of LOCA rod IFA-650.15. In: EHPG HWR-1205. http://uu.diva-portal.org/smash/record.jsf?pid=diva2%3A1143926&dswid=-6370
11. Holcombe S, Andersson P, Svärd SJ, Hallstadius L (2016) Determination of the rod-wise fission gas release fraction in a complete fuel assembly using non-destructive gamma emission tomography. NIM A 837:99–108
12. Andersson P, Holcombe S, Tverberg T (2016) Inspection of a LOCA test rod at the Halden reactor project using gamma emission tomography. In: Top fuel (light water reactor fuel performance meeting)
13. Quirin P (2018) Mirion. Private communication (November 2018)
14. Eberth J, Simpson J (2008) From Ge(Li) detectors to gamma-ray tracking arrays–50 years of gamma spectroscopy with germanium detectors. Prog Part Nucl Phys 60(2):283–337. https://doi.org/10.1016/j.ppnp.2007.09.001
15. Korichi K, Lauritsen T (2019) Tracking γ rays in highly segmented HPGe detectors: a review of AGATA and GRETINA. Eur Phys J A 55:121
16. Paschalis S et al (2019) The performance of the gamma-ray energy tracking in beam nuclear array GRETINA. Nucl Instrum Methods Phys Res Sect A Accel Spectrom Detect Assoc Equip 709:44–55. https://doi.org/10.1016/j.nima.2013.01.009
17. Akkoyun S et al (2012) AGATA—advanced gamma tracking array. Nucl Instrum Methods Phys Sect A Accel Spectrom Detect Assoc Equip 668:26–58. https://doi.org/10.1016/j.nima.2011.11.081
18. Callas JL, Mahoney WA, Varnell LS, Wheaton WA (1993) High-resolution imaging gamma-ray spectroscopy with externally segmented germanium detectors. Rev Sci Instrum 64:143–153
19. Smith DM et al (2002) The RHESSI spectrometer. Sol Phys 210:33–60
20. Steinbach T et al (2017) Compton imaging with a highly-segmented, position-sensitive HPGe detector. Eur Phys J A 53:23. https://doi.org/10.1140/epja/i2017-12214-9
21. Pelowitz DB (2005) MCNPX(TM) user's manual version 2.5.0
22. Berger MJ, Hubbell JH, Seltzer SM, Chang J, Coursey JS, Sukumar R, Zucker DS, Olsen K (2010) XCOM: photon cross sections database. NIST standard reference database 8 (XGAM). https://doi.org/10.18434/T48G6X
23. Gilmore G (2011) Chapter 14: high count rate systems. In: Practical gamma-ray spectrometry, 2nd edn. West Sussex. ISBN-978-0-470-86196-7
24. Peplowski PN et al (2019) Radiation damage and annealing of three coaxial n-type germanium detectors: preparation for spaceflight missions to asteroid 16 Psyche and Mars' moon Phobos. Nucl Instrum Methods Phys Res Sect A Accel Spectrom Detect Assoc Equip 942:162409. https://doi.org/10.1016/j.nima.2019.162409